Monatshefte für Chemie 137, 249–261 (2006)
DOI 10.1007/s00706-006-0436-x

Monatshefte für Chemie
Chemical Monthly
Printed in Austria

Transition Metal Centered Trigonal Prisms as Building Units in Various Rare Earth–Transition Metal-Indides

Vasyl I. Zaremba[1], **Ute Ch. Rodewald**[2], **Mar'yana Lukachuk**[3], **Vitaliy P. Dubenskiy**[1], **Birgit Heying**[2], **Kenichi Katoh**[4], **Yuzuru Niide**[4], **Akira Ochiai**[5], and **Rainer Pöttgen**[2,*]

[1] Inorganic Chemistry Department, Ivan Franko National University, 79005 Lviv, Ukraine
[2] Institut für Anorganische und Analytische Chemie and NRW Graduate School of Chemistry, Westfälische Wilhelms-Universität Münster, 48149 Münster, Germany
[3] Max-Plank-Institut für Festkörperforschung, 70569 Stuttgart, Germany
[4] Department of Applied Physics, National Defense Academy, 239-8686, Yokosuka, Japan
[5] Center for Low Temperature Science, Tohoku University, 980-8578, Sendai, Japan

Received June 30, 2005; accepted August 9, 2005
Published online February 20, 2006

Summary. The rare earth–transition metal-indides GdPdIn, ErPdIn, YbPdIn, YPtIn, TmPtIn, $Dy_4Pd_{10}In_{21}$, $PrPt_2In_2$, and $Tb_2Pt_7In_{16}$ were prepared by arc-melting of the elements or by induction melting of the elements in sealed tantalum tubes in a water-cooled sample chamber of a high-frequency furnace. Single crystals of $Dy_4Pd_{10}In_{21}$ and $Tb_2Pt_7In_{16}$ were grown through special annealing procedures. The indides were investigated *via* X-ray powder diffraction and all structures were refined from X-ray single crystal diffractometer data: ZrNiAl type, $P\bar{6}2m$, $a = 767.8(3)$, $c = 390.7(2)$ pm, $wR2 = 0.0722$, 356 F^2 values for GdPdIn; $a = 766.7(3)$, $c = 376.7(1)$ pm, $wR2 = 0.0433$, 348 F^2 values for ErPdIn; $a = 757.2(2)$, $c = 393.59(8)$ pm, $wR2 = 0.0388$, 434 F^2 values for YbPdIn; $a = 758.2(2)$, $c = 384.95(8)$ pm, $wR2 = 0.0643$, 353 F^2 values for YPtIn; and $a = 753.4(1)$, $c = 376.71(4)$ pm, $wR2 = 0.0844$, 310 F^2 values for TmPtIn, with 14 variable parameters per refinement. $Dy_4Pd_{10}In_{21}$ crystallizes with the monoclinic $Ho_4Ni_{10}Ga_{21}$ structure: $C2/m$, $a = 2284.5(8)$, $b = 441.0(2)$, $c = 1931.4(7)$ pm, $\beta = 132.74(2)^\circ$, $wR2 = 0.0419$, 1690 F^2 values, 112 variable parameters. $PrPt_2In_2$ adopts the $CePt_2In_2$ type: $P2_1/m$, $a = 1013.2(3)$, $b = 447.2(3)$, $c = 1019.5(3)$ pm, $\beta = 116.69(2)^\circ$, $wR2 = 0.0607$, 1259 F^2 values, 63 variable parameters. $Tb_2Pt_7In_{16}$ is the second representative of the orthorhombic $Dy_2Pt_7In_{16}$ type: $Cmmm$, $a = 1211.6(2)$, $b = 1997.1(4)$, $c = 440.52(9)$ pm, $wR2 = 0.0787$, 1341 F^2 values, 45 variable parameters. The common structural motif of the four different structure types are transition metal centered trigonal prisms formed by the rare earth metal and indium atoms. These prisms are condensed *via* common corners or via In–In bonds. The crystal chemistry of the four different structure types is discussed.

Keywords. Rare earth compounds; Indides; Crystal chemistry.

* Corresponding author. E-mail: pottgen@uni-muenster.de

Introduction

The structures of $RE_xT_y\text{In}_z$ indides (RE = rare earth element, T = transition metal) show a large variety of bonding patterns. Those compounds with a high rare earth metal content typically show high coordination numbers and relatively complex structures. If the transition metal content increases, the $RE_xT_y\text{In}_z$ indides show a tendency for transition metal cluster formation and the indium-rich ones often contain distorted *bcc* indium cubes as substructures. The structural chemistry of these materials has been summarized in a recent review [1].

Those $RE_xT_y\text{In}_z$ indides with almost similar x, y, and z values show formation of $[T_y\text{In}_z]$ polyanionic networks which leave cages or channels for the rare earth metal atoms. A common structural motif of their structures is the regular or distorted trigonal prismatic coordination of the transition metal atoms. These trigonal prisms can be built up exclusively by indium or rare earth metal atoms or both of them.

During our recent phase analytical investigations of the *RE*–*T*–In systems *via* indium flux synthesis [2–9], we obtained a series of well-shaped single crystals of various $RE_xT_y\text{In}_z$ indides which contain these trigonal prismatic building units. The synthesis and single crystal X-ray structure refinements of GdPdIn, ErPdIn, YbPdIn, YPtIn, TmPtIn, $PrPt_2In_2$, and the new indides $Dy_4Pd_{10}In_{21}$ and $Tb_2Pt_7In_{16}$ are reported herein. So far, only X-ray powder data have been reported for GdPdIn [10–13], ErPdIn [10, 14–15], YbPdIn [10, 14, 16, 17], YPtIn [18], TmPtIn [18], and $PrPt_2In_2$ [19].

Discussion

The rare earth–transition metal-indides GdPdIn, ErPdIn, YbPdIn, YPtIn, TmPtIn, $Dy_4Pd_{10}In_{21}$, $PrPt_2In_2$, and $Tb_2Pt_7In_{16}$ have been obtained as small single crystals suitable for structure refinements. So far, for GdPdIn, ErPdIn, YbPdIn, YPtIn, TmPtIn, and $PrPt_2In_2$ only X-ray powder data have been reported in literature [10–19]. The indides $Dy_4Pd_{10}In_{21}$ and $Tb_2Pt_7In_{16}$ are reported here for the first time. ErPdIn has been investigated by neutron powder diffraction at low temperature for determination of the magnetic structure. The nuclear structure was refined on the basis of the 15 K data [15], slightly above the magnetic ordering temperature. The single crystal X-ray data of ErPdIn reported herein confirm the neutron data, however, the atomic positions have been determined with a better accuracy.

The common structural motif of all indides reported herein are transition metal centered trigonal prisms. In total we have to discuss four different structure types. The equiatomic compounds crystallize with the hexagonal ZrNiAl type [23–25], $PrPt_2In_2$ adopts the monoclinic $CePt_2In_2$ structure [19], $Dy_4Pd_{10}In_{21}$ the monoclinic $Ho_4Ni_{10}Ga_{21}$ type [30], and $Tb_2Pt_7In_{16}$ is the second representative of the orthorhombic $Dy_2Pt_7In_{16}$ structure [3]. Projections of the YPtIn, $PrPt_2In_2$, $Dy_4Pd_{10}In_{21}$, and $Tb_2Pt_7In_{16}$ structures along the short unit cell axis are shown in Fig. 1.

In the YPtIn structure, the trigonal prisms are exclusively formed either by yttrium or indium atoms. The [Pt2Y$_6$] prisms are condensed *via* edges in the *ab* plane, leading to six-membered rings, which are further condensed in the *c* direction *via* the triangular Y$_3$ faces. Within the large tubes formed by these prisms we observe the Pt1 centered prisms of indium atoms that are shifted with respect to the

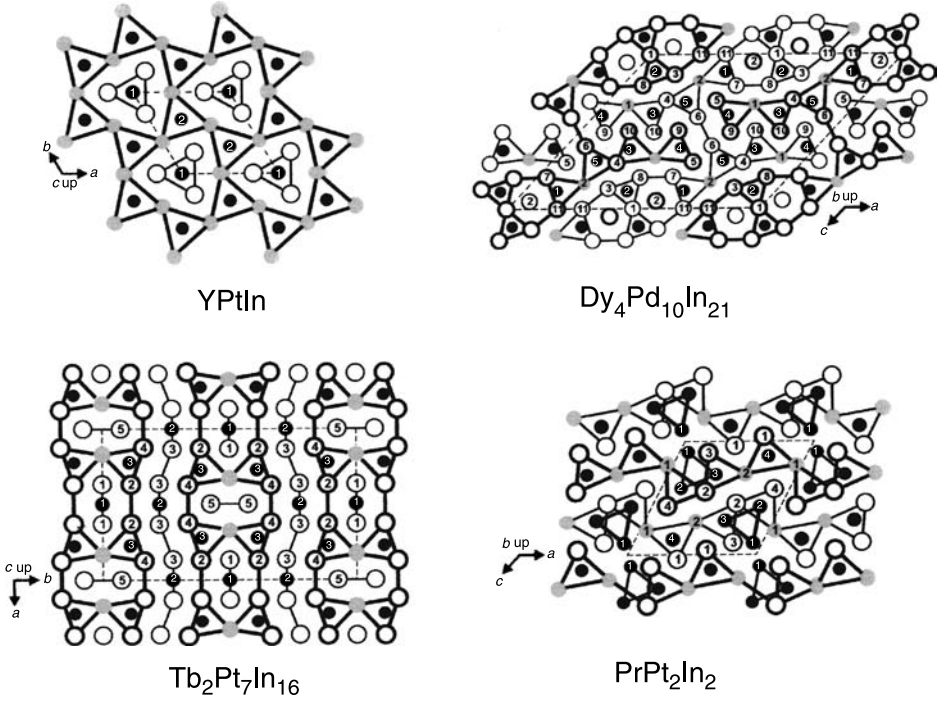

Fig. 1. Projections of the YPtIn, $PrPt_2In_2$, $Tb_2Pt_7In_{16}$, and $Dy_4Pd_{10}In_{21}$ structures along the short unit cell axis; the rare earth, transition metal, and indium atoms are drawn as light grey, black filled, and open circles, respectively; all atoms lie at mirror planes at two different heights perpendicular to the short axis, indicated by thin and thick lines, respectively; the trigonal prisms around the transition metal atoms are emphasized; also the platinum triangles in the $PrPt_2In_2$ structure are drawn

$[Pt2Y_6]$ prisms by half the translation period *c*. The crystal chemistry of ZrNiAl type intermetallics has repeatedly been discussed in literature. For further details we refer to recent review articles [31, 32].

A different condensation pattern is observed for the monoclinic $PrPt_2In_2$ structure (Fig. 1). The platinum sites Pt2, Pt3, and Pt4 occupy $[Pr_4In_2]$ or $[Pr_2In_4]$ prisms. The latter are condensed *via* common edges in the *ac* plane, leading to chains that extend approximately in the *x* direction. The neighbouring chains can be generated *via* the two-fold screw axis. They are shifted by half the *b* translation period, emphasized by thin and thick lines in Fig. 1. The Pt1 atoms are not involved in this trigonal prismatic building unit. Together with the Pt2 and Pt3 atoms they build up triangles at Pt–Pt distances from 282 to 296 pm, only slightly longer than the Pt–Pt distance of 277 pm in *fcc* platinum [33]. From a geometrical point of view, the two Pt1, Pr1, and In3 atoms around the origin of the unit cell form an octahedral void, however, a substantially distorted one that would not be suitable for incorporation of a further small atom. A similar structural motif occurs in $Ho_6Co_{2.135}In_{0.865}$ [34].

Again, in $Dy_4Pd_{10}In_{21}$, all palladium atoms have a trigonal prismatic coordination. Due to the high indium content we observe only two kinds of trigonal prisms, $[Dy_2In_4]$ and $[In_6]$. The rectangular faces of these prisms are all capped by further indium atoms, leading to coordination number 9, typically observed for this kind of intermetallic compounds. The trigonal prisms are condensed *via* common edges

within the *ac* plane. Due to the *C*-centering of the unit cell we observe the condensed building unit of trigonal prisms at two different heights ($y = 0$ and $y = 1/2$). In contrast to the isotypic compounds with the light rare earth atoms [2], $Dy_4Pd_{10}In_{21}$ shows a mixed Pd/In occupancy on the 2*b* site. For reasons of simplicity, we write the ideal formula in the discussion section. The cell volume of the dysprosium compound fits well into the series of $RE_4Pd_{10}In_{21}$ compounds [2, 35], reflecting the lanthanoid contraction. For further crystal chemical details we refer to our previous manuscripts on the series $RE_4Pd_{10}In_{21}$ [2, 35] and $RE_4Pt_{10}In_{21}$ [9].

In the $Tb_2Pt_7In_{16}$ structure, only the Pt3 atoms have a tricapped trigonal prismatic coordination. Due to the large indium content, these prisms are formed by two terbium and four indium atoms. The prisms are condensed *via* the terbium edges to double units and further *via* In–In bonds, leading to one-dimensional strands that extend in the *a* direction. Among the compounds discussed herein, $Tb_2Pt_7In_{16}$ has the far smallest rare earth content. Consequently, not all platinum atoms are in contact with rare earth atoms. One observes an eight-fold indium coordination for the Pt1 and Pt2 atoms. These crystal chemical details are discussed in Ref. [3]. In accordance with the lanthanoid contraction, the cell volume of the terbium compound is slightly larger than that of $Dy_2Pt_7In_{16}$.

The shortest interatomic distances in the structures of YPtIn, $PrPt_2In_2$, $Dy_4Pd_{10}In_{21}$, and $Tb_2Pt_7In_{16}$ occur between the transition metal (*T*) and indium atoms. The *T*–In distances are all close to the sums of the covalent radii [36] for Pd + In and Pt + In. We can thus assume a significant degree of *T*–In bonding in the [PtIn], [Pt_2In_2], [Pd_4In_{10}], and [Pt_7In_{16}] networks. Furthermore one observes also a

Table 1. Lattice parameters of the hexagonal indides *RET*In with ZrNiAl type structure, the monoclinic indide $Dy_4Pd_{10.48(6)}In_{20.52(6)}$ with $Ho_4Ni_{10}Ga_{21}$ type structure, $PrPt_{1.958(5)}In_{2.042(5)}$ with $CePt_2In_2$ type structure, and the orthorhombic indide $Tb_2Pt_7In_{16}$ with $Dy_2Pd_7In_{16}$ type structure

Compound	*a*/pm	*b*/pm	*c*/pm	*β*/°	*V*/nm^3	Reference
GdPdIn	767.8(3)	*a*	390.7(2)	–	0.1995	this work
GdPdIn	764.7	*a*	388.6	–	0.1968	[13]
ErPdIn	766.7(3)	*a*	376.7(1)	–	0.1918	this work
ErPdIn[a]	763.2	*a*	375.4	–	0.1894	[10]
ErPdIn	763.1	*a*	375.5	–	0.1894	[14]
ErPdIn*	763.57(15)	*a*	375.08(10)	–	0.18939	[15]
YbPdIn	757.2(2)	*a*	393.59(8)	–	0.1954	this work
YbPdIn	758.7	*a*	394.1	–	0.1965	[17]
YbPdIn	757.3	*a*	393.3	–	0.1953	[14]
YbPdIn	757.4	*a*	393.2	–	0.1953	[10]
YPtIn	758.2(2)	*a*	384.95(8)	–	0.1916	this work
YPtIn	758.3	*a*	384.6	–	0.1915	[18]
TmPtIn	753.4(1)	*a*	376.71(4)	–	0.1852	this work
TmPtIn	756.0	*a*	378.0	–	0.1871	[18]
$Dy_4Pd_{10.48}In_{20.52}$	2284.5(8)	441.0(2)	1931.4(7)	132.74(2)	1.4289	this work
$PrPt_{1.958}In_{2.042}$	1013.2(3)	447.2(3)	1019.5(3)	116.69(2)	0.4127	this work
$PrPt_2In_2$	1015.2(4)	446.2(1)	1020.4(3)	116.78(2)	0.4168	[19]
$Tb_2Pt_7In_{16}$	1211.6(2)	1997.1(4)	440.52(9)	–	1.0659	this work

* 15 K neutron data

variety of In–In contacts, as expected for such indium-rich intermetallic compounds. The shorter In–In distances in all four indides are shorter or close to the In–In distances in elemental, tetragonal body-centered indium (4×325, 8×338 pm) [33]. Also these In–In interactions play an important role in the complex three-dimensional networks.

Although the four different structures have many common geometrical motifs, there is one significant difference which concerns the bonding of the rare earth metal (*RE*) to the transition metal-indium network. In the structures of YPtIn, $PrPt_2In_2$, and $Tb_2Pt_7In_{16}$, the rare earth metal atoms are connected to the networks through *RE*–Pt contacts, but through *RE*–In contacts in $Dy_4Pd_{10}In_{21}$. For further crystal chemical details we refer to the original literature, where the respective structure types have been discussed first [1–3, 19].

Experimental

Synthesis

Starting materials for the preparation of GdPdIn, ErPdIn, YbPdIn, YPtIn, TmPtIn, $PrPt_2In_2$, $Dy_4Pd_{10}In_{21}$, and $Tb_2Pt_7In_{16}$ were ingots of the rare earth metals (Johnson Matthey, Chempur, or Kelpin), palladium and platinum powder (Degussa-Hüls, *ca.* 200 mesh), and indium tear drops

Table 2. Crystal data and structure refinement for *RE*PdIn (*RE* = Gd, Er, Yb) and YPtIn with ZrNiAl type structure, space group $P\bar{6}2m$; Z = 3

Empirical formula	GdPdIn	ErPdIn	YbPdIn	YPtIn
Molar mass	378.47 g/mol	388.48 g/mol	394.26 g/mol	398.82 g/mol
Unit cell dimensions	Table 1	Table 1	Table 1	Table 1
Calculated density	9.45 g/cm^3	10.09 g/cm^3	10.05 g/cm^3	10.37 g/cm^3
Crystal size	$35 \times 40 \times 70$ μm^3	$20 \times 20 \times 40$ μm^3	$10 \times 40 \times 40$ μm^3	$20 \times 20 \times 80$ μm^3
Detector distance	60 mm	–	–	–
Exposure time	12 min	–	–	–
ω range; increment	0–180°; 1.0°	–	–	–
Integr. param. A, B, EMS	12.8; 2.9; 0.041	–	–	–
Transm. ratio (max/min)	1.97	1.41	2.44	2.48
Absorption coefficient	39.5 mm^{-1}	48.0 mm^{-1}	50.8 mm^{-1}	85.7 mm^{-1}
$F(000)$	477	489	495	498
θ range	3° to 35°	3° to 35°	3° to 40°	3° to 35°
Range in *hkl*	±12, ±12, ±6	±12, ±12, +6	±12, ±12, ±7	±12, ±12, ±6
Total no. reflections	2886	1884	3807	3396
Independent reflections	356 ($R_{int} = 0.046$)	348 ($R_{int} = 0.044$)	434 ($R_{int} = 0.070$)	353 ($R_{int} = 0.045$)
Reflections with $I > 2\sigma(I)$	355 ($R_\sigma = 0.018$)	331 ($R_\sigma = 0.024$)	409 ($R_\sigma = 0.028$)	342 ($R_\sigma = 0.018$)
Data/parameters	356/14	348/14	434/14	353/14
Goodness-of-fit on F^2	1.404	1.191	1.150	0.586
Final R indices [$I > 2\sigma(I)$]	$R1 = 0.0219$	$R1 = 0.0210$	$R1 = 0.0198$	$R1 = 0.0154$
	$wR2 = 0.0722$	$wR2 = 0.0425$	$wR2 = 0.0382$	$wR2 = 0.0600$
R indices (all data)	$R1 = 0.0220$	$R1 = 0.0236$	$R1 = 0.0225$	$R1 = 0.0167$
	$wR2 = 0.0722$	$wR2 = 0.0433$	$wR2 = 0.0388$	$wR2 = 0.0643$
Extinction coefficient	0.020(2)	0.0106(7)	0.011(1)	0.015(2)
Flack parameter	0.02(4)	0.00(2)	0.00(1)	−0.00(2)
Largest diff. peak and hole	1.79/−2.35 e/Å^3	2.31/−2.02 e/Å^3	2.59/−2.38 e/Å^3	1.12/−1.49 e/Å^3

(Johnson Matthey), all with stated purities better than 99.9%). In a first step, the rare earth metal pieces were melted under 600 mbar argon to small buttons in an arc-melting furnace [20]. The argon was purified over titanium sponge (900 K), silica gel, and molecular sieves.

Samples of GdPdIn, ErPdIn, YPtIn, TmPtIn, and $PrPt_2In_2$ were prepared from the elements *via* arc-melting. Pre-melted buttons of the rare earth elements, cold-pressed pellets (Ø 6 mm) of palladium or platinum, and pieces of the indium tear drops were mixed in the ideal atomic ratios (1:1:1 and 1:2:2) and arc-melted under an argon pressure of *ca.* 800 mbar. The resulting buttons were remelted three times in order to ensure homogeneity. The total weight losses after the melting procedures were always smaller than 1 wt.%. The brittle samples show metallic luster. They are stable in air.

The smaller YbPdIn crystals originated from a crystal growth procedure *via* the *Bridgman* technique. An arc-melted PdIn alloy was loaded with pieces of ytterbium lumps in a vacuum sealed tungsten crucible. The latter was heated in a tungsten-mesh heater at 1460°C and pulled down at a rate of 2 mm/h after holding for one hour. More details on the preparation procedure are given in Ref. [17].

A well crystallized sample of $Dy_4Pd_{10}In_{21}$ was prepared by high-frequency melting (Hüttinger Elektronik, Freiburg, Typ TIG 5/300) of the elements in the ideal 4:10:21 ratio in a glassy carbon crucible in a water-cooled sample chamber [21]. Special heat treatment was necessary for the growth of single crystals. The $Dy_4Pd_{10}In_{21}$ crystals were synthesized in a similar way as the polycrystalline sample, but with an excess of indium as a flux. The previously synthesized sample was crushed, mixed

Table 3. Crystal data and structure refinement for TmPtIn, $Dy_4Pd_{10.48(6)}In_{20.52(6)}$, $PrPt_{1.958(5)}In_{2.042(5)}$, and $Tb_2Pt_7In_{16}$

Empirical formula	TmPtIn	$Dy_4Pd_{10.48(6)}In_{20.52(6)}$	$PrPt_{1.958(5)}In_{2.042(5)}$	$Tb_2Pt_7In_{16}$
Structure type	ZrNiAl	$Ho_4Ni_{10}Ga_{21}$	$CePt_2In_2$	$Dy_2Pt_7In_{16}$
Z	3	2	4	2
Molar mass	478.84 g/mol	4123.54 g/mol	752.70 g/mol	3520.59 g/mol
Space group	$P\bar{6}2m$	$C2/m$	$P2_1/m$	$Cmmm$
Unit cell dimensions	Table 1	Table 1	Table 1	Table 1
Calculated density	12.88 g/cm^3	9.58 g/cm^3	12.11 g/cm^3	10.97 g/cm^3
Crystal size	$40\times45\times120$ μm^3	$20\times20\times200$ μm^3	$20\times55\times85$ μm^3	$30\times40\times90$ μm^3
Detector distance	60 mm	60 mm	80 mm	60 mm
Exposure time	14 min	14 min	5 min	18 min
ω range; increment	0–180°; 1.0°	0–180°; 1.0°	0–180°; 1.0°;	0–180°; 1.0°
Integr. param. A, B, EMS	13.9; 2.9; 0.064	14.0; 4.0; 0.016	13.0; 3.0; 0.010	12.5; 3.5; 0.012
Transm. ratio (max/min)	3.79	3.96	6.50	5.91
Absorption coefficient	101.0 mm^{-1}	32.9 mm^{-1}	87.1 mm^{-1}	69.1 mm^{-1}
F(000)	588	3505	1240	2920
θ range	3° to 35°	3° to 35°	2° to 33°	3° to 35°
Range in *hkl*	±11, ±11, ±5	±36, ±7, ±30	±14, ±6, ±15	±19, ±32, ±7
Total no. reflections	1245	4104	4022	7777
Independent reflections	310 ($R_{int}=0.055$)	1690 ($R_{int}=0.026$)	1559 ($R_{int}=0.049$)	1341 ($R_{int}=0.087$)
Reflections with $I>2\sigma(I)$	307 ($R_\sigma=0.033$)	1460 ($R_\sigma=0.022$)	1259 ($R_\sigma=0.048$)	1265 ($R_\sigma=0.046$)
Data/parameters	310/14	1690/112	1259/63	1341/45
Goodness-of-fit on F^2	1.243	1.006	0.970	1.193
Final R indices [$I>2\sigma(I)$]	$R1=0.0317$	$R1=0.0205$	$R1=0.0281$	$R1=0.0337$
	$wR2=0.0842$	$wR2=0.0401$	$wR2=0.0580$	$wR2=0.0773$
R indices (all data)	$R1=0.0322$	$R1=0.0281$	$R1=0.0411$	$R1=0.0365$
	$wR2=0.0844$	$wR2=0.0419$	$wR2=0.0607$	$wR2=0.0787$
Extinction coefficient	0.019(3)	0.00055(3)	0.0097(3)	0.00149(7)
Flack parameter	0.05(3)	–	–	–
Largest diff. peak and hole	3.22/−2.91 e/Å^3	1.02/−1.21 e/Å^3	3.14/−3.86 e/Å^3	4.98/−3.92 e/Å^3

Table 4. Atomic coordinates and isotropic displacement parameters (pm^2) of GdPdIn, ErPdIn, YbPdIn, YPtIn, TmPtIn, $Dy_4Pd_{10.48(6)}In_{20.52(6)}$, $PrPt_{1.958(5)}In_{2.042(5)}$, and $Tb_2Pt_7In_{16}$; U_{eq} is defined as one third of the trace of the orthogonalized U_{ij} tensor

Atom	*Wyck.*	Occ.	*x*	*y*	*z*	U_{eq}
GdPdIn						
Gd	3*g*	1.00	0.5912(1)	0	1/2	136(2)
Pd1	1*b*	1.00	0	0	1/2	119(4)
Pd2	2*c*	1.00	1/3	2/3	0	110(3)
In	3*f*	1.00	0.2548(2)	0	0	117(2)
ErPdIn						
Er	3*g*	1.00	0.40562(8)	0	1/2	123(1)
Pd1	1*b*	1.00	0	0	1/2	101(3)
Pd2	2*c*	1.00	2/3	1/3	0	92(2)
In	3*f*	1.00	0.7408(1)	0	0	93(2)
YbPdIn						
Yb	3*g*	1.00	0.40753(5)	0	1/2	103(1)
Pd1	1*b*	1.00	0	0	1/2	121(2)
Pd2	2*c*	1.00	2/3	1/3	0	120(2)
In	3*f*	1.00	0.74320(8)	0	0	107(1)
YPtIn						
Y	3*g*	1.00	0.4069(2)	0	1/2	74(3)
Pt1	1*b*	1.00	0	0	1/2	86(2)
Pt2	2*c*	1.00	2/3	1/3	0	71(2)
In	3*f*	1.00	0.7410(1)	0	0	77(2)
TmPtIn						
Tm	3*g*	1.00	0.5954(1)	0	1/2	92(3)
Pt1	1*b*	1.00	0	0	1/2	81(3)
Pt2	2*c*	1.00	1/3	2/3	0	86(3)
In	3*f*	1.00	0.2628(2)	0	0	75(3)
$Dy_4Pd_{10.48(6)}In_{20.52(6)}$						
Dy1	4*i*	1.00	0.90222(2)	0	0.67281(2)	95(1)
Dy2	4*i*	1.00	0.70921(2)	0	0.83162(2)	92(1)
Pd1	4*i*	1.00	0.13657(3)	0	0.88548(4)	98(1)
Pd2	4*i*	1.00	0.9126(2)	0	0.8868(1)	113(3)
Pd3	4*i*	1.00	0.26990(3)	0	0.61711(4)	104(1)
Pd4	4*i*	1.00	0.46582(3)	0	0.60634(4)	108(1)
Pd5	4*i*	1.00	0.18196(3)	0	0.69000(4)	94(1)
In1/Pd6	2*b*	0.52(6)/0.48(6)	0	1/2	0	104(2)
In2	8*j*	0.50	0.06346(4)	0.0332(8)	0.95037(5)	121(5)
In3	4*i*	1.00	0.32753(3)	0	0.86981(4)	109(3)
In4	4*i*	1.00	0.76715(3)	0	0.70401(4)	89(1)
In5	4*i*	1.00	0.06680(5)	0	0.69906(7)	87(1)
In6	4*i*	1.00	0.58176(18)	0	0.59411(13)	100(3)
In7	4*i*	1.00	0.54228(3)	0	0.79465(4)	92(1)

(*continued*)

Table 4 (*continued*)

Atom	*Wyck.*	Occ.	*x*	*y*	*z*	U_{eq}
In8	4*i*	1.00	0.41452(6)	0	0.79922(9)	115(2)
In9	4*i*	1.00	0.10639(3)	0	0.50528(4)	93(1)
In10	4*i*	1.00	0.69870(3)	0	0.49665(4)	85(1)
In11	4*i*	1.00	0.70051(3)	0	0.00036(4)	89(1)
$PrPt_{1.958(5)}In_{2.042(5)}$						
Pr1	2*e*	1.00	0.04862(9)	1/4	0.78965(8)	104(2)
Pr2	2*e*	1.00	0.40162(8)	1/4	0.71050(8)	83(2)
Pt1/In5	2*e*	0.92(1)/0.08(1)	0.06955(7)	1/4	0.09964(6)	121(2)
Pt2	2*e*	1.00	0.15742(6)	1/4	0.41856(5)	96(1)
Pt3	2*e*	1.00	0.37334(6)	1/4	0.29693(5)	86(1)
Pt4	2*e*	1.00	0.70591(6)	1/4	0.13187(5)	92(1)
In1	2*e*	1.00	0.4053(1)	1/4	0.0405(1)	86(2)
In2	2*e*	1.00	0.6454(1)	1/4	0.5526(1)	91(2)
In3	2*e*	1.00	0.7725(1)	1/4	0.8958(1)	97(2)
In4	2*e*	1.00	0.8814(1)	1/4	0.4249(1)	86(2)
$Tb_2Pt_7In_{16}$						
Tb	4*h*	1.00	0.83000(5)	0	1/2	95(1)
Pt1	2*c*	1.00	1/2	0	1/2	99(1)
Pt2	4*j*	1.00	0	0.27550(2)	1/2	84(1)
Pt3	8*p*	1.00	0.27595(3)	0.39006(2)	0	107(1)
In1	4*g*	1.00	0.63179(7)	0	0	99(2)
In2	8*q*	1.00	0.13012(5)	0.38670(3)	1/2	97(1)
In3	8*p*	1.00	0.13457(5)	0.27633(3)	0	124(1)
In4	8*q*	1.00	0.12487(5)	0.16327(3)	1/2	121(1)
In5	4*i*	1.00	0	0.92626(4)	0	108(2)

with a 10 wt.% excess of indium, and placed in a glassy carbon crucible. Next, the crucible was slowly heated in an induction furnace in an atmosphere of flowing argon up to 1340 K. The sample was kept at that temperature for 30 minutes, then slowly cooled to 1040 K within 4 hours, and finally the furnace was turned off. The temperature was controlled through a Sensor Therm Metis MS09 pyrometer with an accuracy of ± 30 K. The sample could easily be separated from the crucible and no reaction of the sample with the crucible material could be detected. Single crystals and fine grained powders of $Dy_4Pd_{10}In_{21}$ are stable in moist air.

Single crystals of $Tb_2Pt_7In_{16}$ were grown in an indium flux. In a first step, an alloy of composition $TbPt_3In_6$ was obtained *via* arc-melting as described above. In a second step, the $TbPd_3In_6$ button was crushed, powdered in a steel mortar and cold-pressed to a pellet. The pellet, with an excess of 10 wt.% indium, was placed in a tantalum container and sealed in an evacuated silica tube which was placed in a muffle furnace. The ampoule was first heated to 1270 K within 6 hours and held at that temperature for another 6 hours. Next, the temperature was lowered at a rate 5 K/h to 970 K, then at a rate 10 K/h to 670 K, and finally cooled to room temperature within 10 hours. After cooling to room temperature, the sample could easily be separated from the tantalum container. No reaction of the sample with the crucible material could be detected.

Scanning Electron Microscopy

The single crystals investigated on the diffractometer have been analyzed by EDX measurements using a LEICA 420 I scanning electron microscope with the rare earth trifluorides, palladium, platinum, and

indium arsenide as standards. No impurity elements were detected. Various point analyses on the crystals were in good agreement with the ideal compositions determined by the single crystal X-ray data.

X-Ray Film Data and Structure Refinements

The polycrystalline samples were characterized through *Guinier* powder patterns using CuKα_1 radiation and α-quartz ($a = 491.30$, $c = 540.46$ pm) as an internal standard. The *Guinier* camera was equipped with an imaging plate system (Fujifilm BAS-1800). The lattice parameters (Table 1) were deduced from least-squares fits of the powder data. To ensure correct indexing, the experimental

Table 5. Interatomic distances (pm), calculated with the powder lattice parameters of YPtIn and $PrPt_{1.958}In_{2.042}$; standard deviations are all equal or less than 0.2 pm; all distances within the first coordination spheres are listed; $M = 92(1)\%$ Pt + 8(1)% In

YPtIn										
Y:	4	Pt2	299.9	Pt1:	6	In	275.0	In1:	2	Pt1	275.0
	1	Pt1	308.5		3	Y	308.5		2	Pt2	285.1
	2	In	318.1	Pt2:	3	In	285.1		2	Y	318.1
	4	In	332.0		6	Y	299.9		4	Y	332.0
	2	Y	385.0						2	In	340.2
	4	Y	398.3								
$PrPt_{1.958}In_{2.042}$										
Pr1:	2	*M*	298.7	Pt2:	1	In4	282.6	In2:	2	Pt3	276.6
	1	*M*	307.1		2	In4	287.5		1	Pt3	281.8
	2	Pt2	314.4		1	Pr2	289.2		2	Pt2	292.4
	2	Pt4	316.8		2	In2	292.4		1	In3	313.9
	1	In4	332.2		1	Pt3	296.0		1	In4	319.5
	1	In1	336.1		1	*M*	296.0		2	Pr2	335.8
	2	In4	341.8		2	Pr1	314.4		2	In2	346.4
	1	In3	342.3	Pt3:	2	In2	276.6		1	Pr2	350.3
	2	In3	365.3		1	In1	277.5		1	Pr1	369.6
	1	In2	369.6		1	In2	281.8	In3:	2	*M*	273.8
Pr2:	1	Pt2	289.2		1	*M*	282.1		1	Pt4	277.6
	2	Pt4	321.6		2	In3	290.5		1	Pt1	278.5
	2	Pt3	321.9		1	Pt2	296.0		2	Pt3	290.5
	2	In1	328.8		2	Pr2	321.9		2	In1	311.7
	1	In1	334.8	Pt4:	1	In4	270.5		1	In2	313.9
	2	In2	335.8		2	In1	275.3		1	Pr2	336.4
	1	In3	336.4		1	In1	275.6		1	Pr1	342.3
	2	In4	340.2		1	In3	277.6		2	Pr1	365.3
	1	In2	350.3		2	Pr1	316.8	In4:	1	Pt4	270.5
M:	2	In3	273.8		2	Pr2	321.6		1	Pt2	282.6
	1	In3	278.5	In1:	2	Pt4	275.3		2	Pt2	287.5
	1	Pt3	282.1		1	Pt4	275.6		2	In4	313.3
	2	*M*	292.3		1	Pt3	277.5		1	In2	319.5
	1	Pt2	296.0		2	In3	311.7		1	Pr1	332.2
	2	Pr1	298.7		2	In1	328.5		2	Pr2	340.2
	1	Pr1	307.1		2	Pr2	328.8		2	Pr1	341.8
					1	Pr2	334.8				
					1	Pr1	336.1				

powder patterns were compared with calculated ones [22] using the atomic positions obtained from the structure refinements. The lattice parameters derived here are in good agreement with the literature data (see Table 1).

Small single crystals of GdPdIn, ErPdIn, YbPdIn, YPtIn, TmPtIn, $Dy_4Pd_{10}In_{21}$, $PrPt_2In_2$, and $Tb_2Pt_7In_{16}$ were selected from the crushed samples. Most crystals were needle or lath shaped. They were examined by *Laue* photographs on a *Buerger* precession camera (equipped with an imaging plate system Fujifilm BAS-1800) in order to establish suitability for intensity data collection. Intensity data of ErPdIn, YbPdIn, and YPtIn were recorded at room temperature by use of a four-circle diffractometer (CAD4) with graphite monochromatized MoKα radiation ($\lambda = 71.073$ pm) and a scintillation counter with pulse-height discrimination. The scans were taken in the $\omega/2\theta$ mode and empirical absorption corrections were applied on the basis of psi-scan data followed by spherical absorption corrections. The GdPdIn, TmPtIn, $Dy_4Pd_{10}In_{21}$, $PrPt_2In_2$, and $Tb_2Pt_7In_{16}$ crystals were measured at room temperature on a Stoe IPDS-II diffractometer with graphite monochromatized MoKα radiation. A numerical absorption correction was applied to these data. All relevant crystallographic details for the data collections and evaluations are listed in Tables 2 and 3.

Careful examination of the GdPdIn, ErPdIn, YbPdIn, YPtIn, and TmPtIn data sets revealed space group $P\bar{6}2m$ and isotypism with ZrNiAl [23–25]. The atomic positions of SmRhIn [26] were taken as starting values and the structures were refined using SHELXL-97 (full-matrix least-squares on F_o^2) [27] with anisotropic atomic displacement parameters for all sites. Refinement of the correct absolute structure was ensured through refinement of the *Flack* parameter [28, 29]. None of the crystals showed twinning by inversion. The occupancy parameters were refined in separate series of least-squares cycles. All sites were fully occupied within two standard deviations and in the final cycles the ideal values were assumed again.

The $PrPt_2In_2$ data set was compatible with space group $P2_1/m$, in agreement with earlier investigations on $CePt_2In_2$ [19]. The atomic parameters of the cerium compound were taken as starting model and the structure was refined with anisotropic displacement parameters for all atoms. In contrast to

Table 6. Interatomic distances (pm), calculated with the powder lattice parameters of $Tb_2Pt_7In_{16}$; standard deviations are all equal or less than 0.1 pm; all distances within the first coordination spheres are listed

Tb:	4	Pt3	317.8	In1:	2	Pt1	272.1	In3:	2	Pt2	274.0
	2	In1	325.9		2	Pt3	280.6		1	Pt3	284.5
	2	In4	330.6		4	In2	315.8		1	In3	298.8
	2	In2	331.4		1	In1	319.4		2	In2	311.7
	4	In5	335.6		2	Tb	325.9		2	In4	315.7
	1	Pt1	399.8	In2:	1	Pt2	272.3		1	In3	326.1
Pt1:	4	In1	272.1		1	Pt1	275.8	In4:	1	Pt2	270.4
	4	In2	275.8		2	Pt3	282.5		2	Pt3	272.6
	2	Tb	399.8		2	In3	311.7		1	In4	302.6
Pt2:	2	In4	270.4		1	In4	313.2		1	In2	313.2
	2	In2	272.3		1	In2	315.3		2	In3	315.7
	4	In3	274.0		2	In1	315.8		2	In5	321.5
Pt3:	2	In4	272.6		1	Tb	331.4		1	Tb	330.6
	1	In1	280.6					In5:	2	Pt3	280.9
	1	In5	280.9						1	In5	294.6
	2	In2	282.5						4	In4	321.5
	1	In3	284.5						4	Tb	335.6
	2	Tb	317.8								

Table 7. Interatomic distances (pm), calculated with the powder lattice parameters of $Dy_4Pd_{10.48(6)}In_{20.52(6)}$; standard deviations are all equal or less than 0.3 pm; all distances within the first coordination spheres are listed; the distances drawn in italics are affected by the In 2 split position; the *M* site is occupied by 48(6)% Pd and 52(6)% In

Dy1:	2	In8	315.8	Pd1:	2	*In2*	*268.8*	Pd5:	1	In9	271.1
	2	In7	322.8		2	In7	273.0		1	In3	272.8
	2	In10	326.3		2	In11	274.2		1	In5	275.3
	2	Pd3	327.8		1	In11	275.2		2	In6	278.9
	1	In9	330.9		1	In5	277.7		2	In4	283.0
	2	Pd4	334.0		2	Dy2	332.3		1	Pd3	314.0
	1	In10	342.4	Pd2:	1	In4	275.4		2	Dy2	322.8
	1	In5	343.6		*2*	*In2*	*276.9*	*M*:	4	Pd2	277.6
	1	In4	352.3		2	*M*	277.6		2	In3	289.8
	2	*In2*	*394.0*		2	In8	279.8		2	In8	292.8
Dy2:	2	In3	316.3		*2*	*In2*	*280.6*		*4*	*In2*	*302.4*
	2	Pd5	322.8		2	In3	280.7		*4*	*In2*	*323.1*
	2	In11	325.0		1	Pd2	337.1	*In2:*	*1*	*In2*	*29.3*
	2	In5	327.1	Pd3:	1	In10	273.5		*1*	*Pd1*	*268.8*
	2	Pd1	332.3		1	In8	274.1		*1*	*Pd2*	*276.8*
	1	In7	337.0		1	In9	276.9		*1*	*Pd2*	*280.6*
	1	In6	337.5		2	In10	279.0		*1*	*M*	*302.4*
	1	In11	339.7		2	In4	279.8		*1*	*M*	*323.1*
	1	In4	350.1		1	Pd5	314.0		*1*	*In3*	*328.1*
	2	*In2*	*387.8*		2	Dy1	327.8		*1*	*In8*	*329.5*
				Pd4:	2	In9	272.1		*1*	*In11*	*329.7*
					1	In7	276.7		*1*	*In7*	*339.7*
					2	In5	279.0		*1*	*In3*	*347.2*
					1	In6	281.4		*1*	*In8*	*348.5*
					1	In10	281.7		*1*	*In11*	*348.7*
					1	In6	323.4		*1*	*In7*	*358.2*
					2	Dy1	334.0		*1*	*Dy2*	*387.8*
									1	*Dy1*	*394.0*
In3:	1	Pd5	272.8	In6:	2	Pd5	278.9	In9:	1	Pd5	271.1
	2	Pd2	280.7		1	Pd4	281.4		2	Pd4	272.1
	1	*M*	289.8		1	In6	295.6		1	Pd3	276.9
	1	In11	298.0		2	In9	307.1		2	In6	307.1
	1	In8	308.0		2	In5	316.7		2	In10	313.3
	2	Dy2	316.3		1	In4	320.0		1	In5	316.8
	2	*In2*	*328.1*		1	Pd4	323.4		1	Dy1	330.9
	2	In4	332.0		1	Dy2	337.5	In10:	1	Pd3	273.5
	2	*In2*	*347.2*	In7:	2	Pd1	273.0		2	Pd3	279.0
In4:	1	Pd2	275.4		1	Pd4	276.7		1	Pd4	281.7
	2	Pd3	279.8		1	In8	297.9		2	In9	313.3
	2	Pd5	283.0		1	In11	305.9		2	In10	315.6
	1	In10	316.0		2	In5	316.0		1	In4	316.0
	1	In6	320.0		2	Dy1	322.8		2	Dy1	326.3
	2	In3	332.0		1	Dy2	337.0		1	Dy1	342.4
	2	In8	334.3		*2*	*In2*	*339.7*	In11:	2	Pd1	274.2
	1	Dy2	350.1		*2*	*In2*	*358.2*		1	Pd1	275.2
	1	Dy1	352.3	In8:	1	Pd3	274.1		1	In3	298.0
In5:	1	Pd5	275.3		2	Pd2	279.8		1	In7	305.9
	1	Pd1	277.7		1	*M*	292.8		2	In11	316.5
	2	Pd4	279.0		1	In7	297.9		2	Dy2	325.0
	2	In7	316.0		1	In3	308.0		2	In2	329.7
	2	In6	316.7		2	Dy1	315.8		1	Dy2	339.7
	1	In9	316.8		*2*	*In2*	*329.5*		*2*	*In2*	*348.7*
	2	Dy2	327.1		2	In4	334.3				
	1	Dy1	343.6		*2*	*In2*	*348.5*				

$CePt_2In_2$, refinement of the occupancy parameters revealed a mixed Pt1/In5 occupancy for the praseodymium compound, leading to a refined composition $PrPt_{1.958(5)}In_{2.042(5)}$ for the investigated single crystal. Although the equivalent isotropic displacement parameter of 121(2) pm^2 for the mixed Pt1/In5 position is somewhat high, there is no pronounced anisotropic displacement: $U_{11} = 101(3)$, $U_{22} = 121(3)$, and $U_{33} = 112(3)$ pm^2.

The $Dy_4Pd_{10}In_{21}$ diffraction data revealed a monoclinic cell and the systematic extincitions were only those for a *C*-centered lattice. In agreement with the earlier work on $RE_4Pd_{10}In_{21}$ (RE = La, Ce, Pr, Nd, Sm) [2], space group $C2/m$ was found to be the correct one during the structure refinements. The atomic parameters of $Sm_4Pd_{10}In_{21}$ [2] were taken as starting values and the structure was refined with anisotropic displacement parameters for all sites. Similar to the series of $RE_4Pt_{10}In_{21}$ [9] indides, also the In2 site of $Dy_4Pt_{10}In_{21}$ showed an extremely large U_{22} parameter, indicating local violation of the mirror plane. Since no superstructure reflections have been detected for this crystal, we refined the In2 site isotropically with a split position *xyz* instead *x*0*z*. Refinement of the occupancy parameters revealed a mixed Pd/In occupancy for the 2*b* site, leading to the composition $Dy_4Pd_{10.48(6)}In_{20.52(6)}$ for the investigated single crystal. The origin of the mixed occupancies of the 2*b* sites in these indides is discussed in detail in Refs. [2] and [9].

The data set of $Tb_2Pt_7In_{16}$ showed a *C*-centered orthorhombic lattice and no further extinctions. Space group *Cmmm* was confirmed during the structure refinement. The atomic positions of $Dy_2Pt_7In_{16}$ [3] were taken as the starting model and also this structure was refined with anisotropic displacement parameters for all atoms. The sites were fully occupied. Final difference *Fourier* synthesis revealed no significant residual peaks (see Tables 2 and 3). The highest residual densities, especially for the platinum compounds were all close to the platinum sites and can most likely be attributed to absorption effects. The positional parameters and interatomic distances are listed in Tables 4–7. Further details on the structure refinements are available at Fachinformationszentrum Karlsruhe, D-76344 Eggenstein-Leopoldshafen (Germany), by quoting the Registry Nos. CSD-415506 (GdPdIn), CSD-415507 (ErPdIn), CSD-415508 (YbPdIn), CSD-415509 (YPtIn), CSD-415510 (TmPtIn), CSD-415511 ($Dy_4Pd_{10.48}In_{20.52}$), CSD-415512 ($PrPt_{1.958}In_{2.042}$), and CSD-415513 ($Tb_2Pt_7In_{16}$).

Acknowledgements

We thank *H.-J. Göcke* for the work at the scanning electron microscope. This work was financially supported by the Deutsche Forschungsgemeinschaft. *V.I.Z.* is indebted to the Alexander-von-Humboldt Foundation for a research stipend and *M.L.* to the NRW Graduate School of Chemistry for a PhD stipend.

References

[1] Kalychak YaM, Zaremba VI, Pöttgen R, Lukachuk M, Hoffmann R-D (2005) Rare Earth–Transition Metal-Indides. In: Gschneidner KA Jr, Pecharsky VK, Bünzli J-C, Handbook on the Physics and Chemistry of Rare Earths, Elsevier, Amsterdam, Vol. 34, chapter 218, 1–133

[2] Zaremba VI, Rodewald UCh, Kalychak YaM, Galadzhun YaV, Kaczorowski D, Hoffmann R-D, Pöttgen R (2003) Z Anorg Allg Chem **629**: 434

[3] Zaremba VI, Kalychak YaM, Dubenskiy VP, Hoffmann R-D, Rodewald UCh, Pöttgen R (2002) J Solid State Chem **169**: 118

[4] Rodewald UCh, Zaremba VI, Galadzhun YaV, Hoffmann R-D, Pöttgen R (2002) Z Anorg Allg Chem **628**: 2293

[5] Zaremba VI, Kalychak YaM, Tyvanchuk YuB, Hoffmann R-D, Möller MH, Pöttgen R (2002) Z Naturforsch **57b**: 791

[6] Zaremba VI, Dubenskiy VP, Kalychak YaM, Hoffmann R-D, Pöttgen R (2002) Solid State Sci **4**: 1293

[7] Zaremba VI, Rodewald UCh, Hoffmann R-D, Kalychak YaM, Pöttgen R (2003) Z Anorg Allg Chem **629**: 1157
[8] Zaremba VI, Rodewald UCh, Pöttgen R (2003) Z Naturforsch **58b**: 805
[9] Zaremba VI, Hlukhyy V, Rodewald UCh, Pöttgen R (2005) Z Anorg Allg Chem **631**: 1371
[10] Ferro R, Marazza R, Rambaldi G (1974) Z Metallkd **65**: 37
[11] de Vries JWC, Thiel RC, Buschow KHJ (1985) J Less-Common Met **111**: 313
[12] Bałanda M, Szytuła A, Guillot M (2002) J Magn Magn Mater **247**: 345
[13] Buschow KHJ (1975) J Less-Common Met **39**: 185
[14] Cirafici S, Palenzona A, Canepa F (1985) **107**: 179
[15] Gondek Ł, Baran S, Szytuła A, Kaczorowski D, Hernández-Velasco J (2005) J Magn Magn Mater **285**: 272
[16] Zell W, Pott R, Roden B, Wohlleben D (1981) Solid State Commun **40**: 751
[17] Katoh K, Terui G, Niide Y, Yoshii S, Kindo K, Oyamada A, Shirakawa M, Ochiai A (2003) J Alloys Compd **360**: 225
[18] Ferro R, Marazza R, Rambaldi G (1974) Z Anorg Allg Chem **410**: 219
[19] Zaremba V, Galadzhun Ya, Kalychak Ya, Kaczorowski D, Stepien-Damm J (2000) J Alloys Compd **296**: 280
[20] Pöttgen R, Gulden Th, Simon A (1999) GIT Labor Fachzeitschrift **43**: 133
[21] Kußmann D, Hoffmann R-D, Pöttgen R (1998) Z Anorg Allg Chem **624**: 1727
[22] Yvon K, Jeitschko W, Parthé E (1977) J Appl Crystallogr **10**: 73
[23] Krypyakevich PI, Markiv VYa, Melnyk EV (1967) Dopov Akad Nauk Ukr RSR, Ser A 750
[24] Dwight AE, Mueller MH, Conner RA Jr, Downey JW, Knott H (1968) Trans Met Soc AIME **242**: 2075
[25] Zumdick MF, Hoffmann R-D, Pöttgen R (1999) Z Naturforsch **54b**: 45
[26] Lukachuk M, Zaremba VI, Pöttgen R (2003) Intermetallics **11**: 581
[27] Sheldrick GM (1997) SHELXL-97, Program for Crystal Structure Refinement, University of Göttingen
[28] Flack HD, Bernadinelli G (1999) Acta Crystallogr **55A**: 908
[29] Flack HD, Bernadinelli G (2000) J Appl Crystallogr **33**: 1143
[30] Grin YuN, Yarmolyuk YaP, Gladyshevskii EI (1979) Dokl Akad Nauk SSSR **245**: 1102
[31] Parthé E, Gelato L, Chabot B, Penzo M, Cenzual K, Gladyshevskii RE (1993) TYPIX – Standardized Data and Crystal Chemical Characterization of Inorganic Structure Types, in Gmelin Handbook of Inorganic and Organometallic Chemistry, 8th edn., Springer
[32] Zumdick MF, Pöttgen R (1999) Z Kristallogr **214**: 90
[33] Donohue J (1974) The Structures of the Elements. Wiley, New York
[34] Kalychak JM, Zaremba VI, Zavalij PY (1993) Z Kristallogr **208**: 380
[35] Łątka K, Zaremba VI, Rodewald UCh, Pöttgen R (2005) unpublished results
[36] Emsley J (1998) The Elements. Oxford University Press